2006

Nonintrusive Mapping Of Near-Surface Preferential Flow

R. S. Freeland
University of Tennessee, Knoxville

Lameck O. Odhiambo
University of Nebraska-Lincoln, lodhiambo2@unl.edu

J. S. Tyner
University of Tennessee, Knoxville

J. T. Ammons
University of Tennessee, Knoxville

W. C. Wright
University of Tennessee, Knoxville

NONINTRUSIVE MAPPING OF NEAR-SURFACE PREFERENTIAL FLOW

R. S. Freeland, L. O. Odhiambo, J. S. Tyner, J. T. Ammons, W. C. Wright

ABSTRACT. *A unique survey protocol has been developed that maps near-subsurface preferential flow using integrated ground-penetrating radar (GPR) and a differential geographical positioning system (DGPS). The survey protocol consists of a mobile GPR system that spirals outward along a prescribed course, continuously gathering subsurface data for an extended period. Metered water is applied to a centrally located water-ponding ring, after first capturing the initial dry-state pattern signatures. The water radiates outward beneath the surface as it follows preferential flow pathways, which the GPR instrumentation spiraling above highlights. After data are collected, pre- and post-water time-elapsed images profiles are segmented by pattern dissimilarities. The specific locales that exhibit pattern shifts from the initial dry state are identified as dynamic water movement. Locales that exhibit pattern shifts are mapped to indicate the rate and direction of preferential flow about the near surface.*

Keywords. *Geophysics, Ground-penetrating radar (GPR), Preferential flow, Soil.*

Researchers are increasingly using ground-penetrating radar (GPR) techniques for a variety of water-related subsurface investigations, such as locating the groundwater table (Shih et al., 1986; Freeland et al., 1998; Nakashima et al., 2001), estimating the soil water content (Chanzy et al., 1996; van Overmeeren et al., 1997; Weiler et al., 1998; Huisman et al., 2001, 2003; Lunt et al., 2005), mapping wetting front movement (Vellidis et al., 1990; Trinks et al., 2001; Lu and Sato, 2002), and identifying preferential flow pathways through which contaminant-loaded water may flow (Freeland et al., 2002a; Gish et al., 2002). Although GPR has been successfully used to detect the movement and distribution of water in the subsurface, it has several drawbacks when applied for such purposes. A major drawback is that GPR data sets collected during a routine field-scale survey are massive. Interpretation by visual inspection is difficult, laborious, tedious, and subjective.

In spite of the drawbacks, GPR is adaptable for rapid, noninvasive subsurface investigation and monitoring over large acreages, as computing power and data capacity increases. Various studies have been conducted to solve some of the drawbacks associated with GPR data interpretation. For example, studies report on employing automated methods for rapid characterization of GPR data (Al-Nuaimy et al., 2000; Shihab et al., 2002, Odhiambo et al., 2004).

Article was submitted for review in March 2005; approved for publication by the Information & Electrical Technologies Division of ASABE in January 2006.

The authors are **Robert S. Freeland, ASABE Member Engineer,** Professor, **Lameck O. Odhiambo, ASABE Member Engineer,** Post-Doctoral Research Associate, **John S. Tyner, ASABE Member Engineer,** Assistant Professor, **John T. Ammons,** Professor, and **Wesley C. Wright, ASABE Member Engineer,** Research Associate, Biosystems Engineering and Environmental Science Department, The University of Tennessee, Knoxville, Tennessee. **Corresponding author:** Robert S. Freeland, Biosystems Engineering and Environmental Science Department, 2506 E. J. Chapman Dr., Knoxville, TN 37996-4531; phone: 865-974-7140; fax: 865-974-4514; e-mail: rfreelan@utk.edu.

Our survey sites reside primarily on Major Land Resource Area 134 (MLRA 134 - Southern Mississippi Valley Silty Uplands), which extends along the Mississippi River from southern Illinois to northern Louisiana (fig. 1). A majority of these lands is in row-crop production, and represent thousands of hectares of soils that formed in the loess-covered Tertiary-aged Claiborne and Wilcox geologic formations (Hardeman, 1966). An interface between the loess and the underlying paleosol (Clay and Coastal Sands) that forms a distinct textural discontinuity at a depth of approximately 2 m occurs in this region (fig. 2). Preferential flow down to and atop this interface is presumed to create transient-saturated conditions that greatly influence, but do not totally control, the near-surface lateral movement of water. Therefore, the objective of the project was to develop a tool that determines the rate and direction of preferential flow about this interface.

SURVEY PROTOCOL

Traditional radargrams (GPR images) taken during wet field conditions have revealed that field regions having

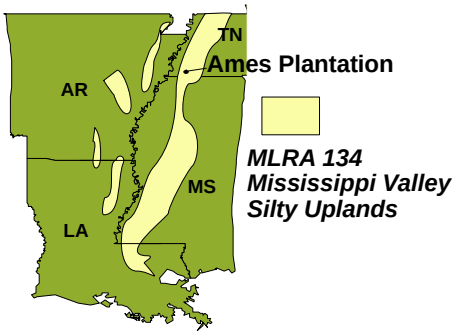

Figure 1. Water quality research site at Ames Plantation and position within Major Land Resource Area 134.

  ISSN 0883−8542

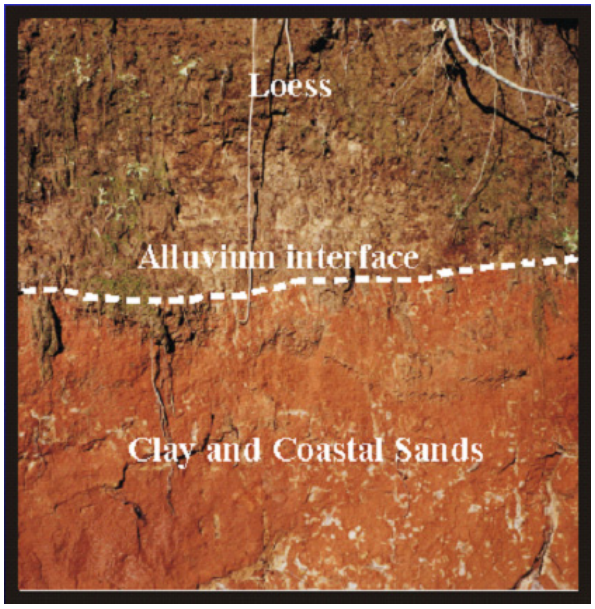

Figure 2. Soil horizon interface approximately 2-m beneath the surface

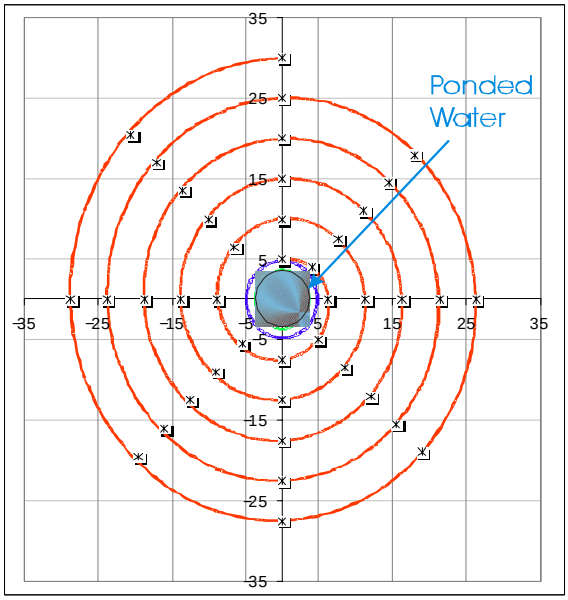

Figure 4. Course guidance layout design showing flag placement.

higher occurrences of macropores and E (eluvial) bodies, which typify vertical preferential flow at this site, had higher occurrences of columnar features in the radargram (Freeland et al., 2002a). More pronounced, thicker horizontal banding near the surface equated to lesser occurrences of vertical preferential flow (Inman et al., 2002). These findings were physically verified both by soil cores and by traditional soil examination through excavating a 4-m deep trench along the original traverse.

Conducting a high-resolution GPR survey generates large amounts of data. Gigabytes of GPR imagery per hectare are obtained while traveling the lengthy, closely spaced traverses that are required in detecting preferential flow pathways (e.g., a 60-m diameter plot required an 8-km long spiraling traverse.) Thus, it is inconceivable to employ high-resolution GPR mapping over entire watersheds if relying upon manual radargram interpretations (fig. 3). For this reason, we employ a Neural Network (NN) classifier to automatically segment patterns based upon similarity (Odhiambo et al., 2004), and to spatially map these identifiers by corresponding geospatial position.

Figure 4 illustrates the survey layout of one such 60-m diameter calibration plot on which a double-ring infiltrometer (10-m diameter outer and 8-m diameter inner rings) is installed. A mobile GPR platform (fig. 5), described by Freeland et al. (2002b), follows an outwardly spiraling traverse from the infiltrometer, the operator guided by survey flags and tracked by a differential global positioning system (DGPS). Multiple baseline "dry" radar imagery are gathered prior to water application for registering spatially-referenced

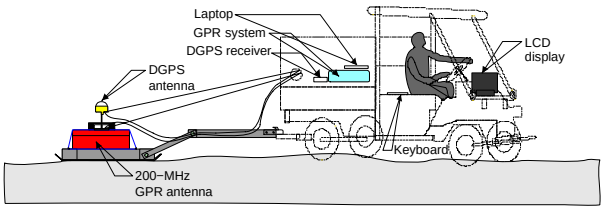

Figure 5. The University of Tennessee Mobile GPR system (Freeland et al., 2002b).

digital signatures of the subsurface, after which water application begins to the infiltrometer at controlled application rates (fig. 6). The data gathering using the mobile platform about the spiral remains continuous.

Mobile GPR System

Equipment components are: 1) a GPR system unit and antenna, 2) a DGPS system for real-time positional data, and 3) an all-terrain utility vehicle:

- SIR System 20™ (GSSI, Inc., North Salem, N.H.) is coupled by an antenna control cable to a 200-MHz antenna (GSSI Model 5106), which provided the desired resolution and penetration depth for the site's soil conditions. Instrument settings and operating parameters are given in table 1.
- A WASS-enabled DGPS receiver (GeoXT™, Trimble Navigation Limited, Sunnydale, Calif.) for fast satellite acquisition and precise tracking, measuring geographical location with sub-meter resolution. One-second data

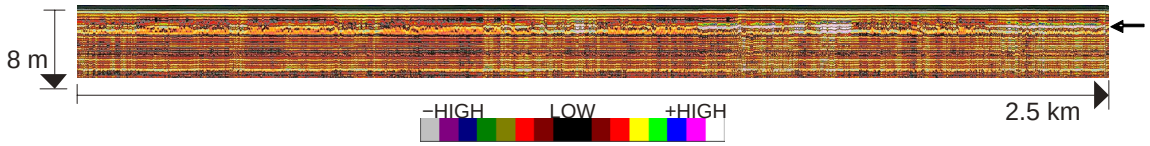

Figure 3. Raw GPR data of a single spiral track unrolled (representing subsurface profile 2.5 km long × 8 m deep). Arrow at right margin points to alluvium interface horizon 2 m beneath surface (fig. 2), of which figure 7 is a top-down view.

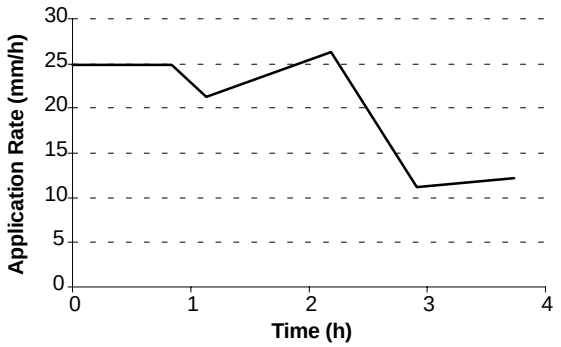

Figure 6. Water application rate (mm/h) of figure 7 within 8-m diameter inner ring.

streams of differentially corrected geographical coordinates are each linked by the SIR-20 GPR system to a corresponding radar scan.

- Kawasaki Mule Model 2510 (Kawasaki Motors Corp., Irvine, Calif.). The four-wheel drive utility vehicle has a four-stroke, 617-cc gasoline engine with electronic ignition, and supplied sufficient electrical power (720 VA) for all instrumentation components from its optional, add-on alternator.

Image Classifier

Water is not easily recognized within a complex GPR image. The challenge is to distinguish between the myriad of GPR reflection patterns caused by the pre-existing dry static conditions and those reflections caused by the imposed water movement. Our approach is to compare the initial dry state image from each subsequent image obtained during water application. Significant pattern changes progressing outward, which are not registered within any of the prior dry state images, are attributed to the large mass of water that is moving into the ground and outward from the central infiltration cell.

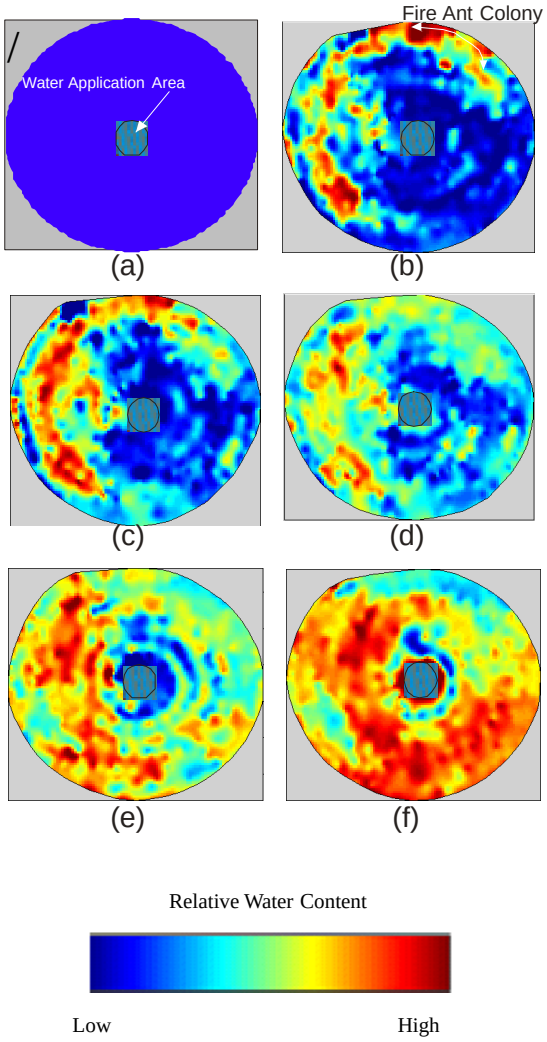

Figure 7. Top-down view of a ≈ 5-cm thick horizontal slice immediately atop the alluvium interface depicting movement from the initial state (a) in 45-min. sequential steps (b-f).

Results and Discussion

Figure 7 presents seven sequential frames (a-f) illustrating GPR signal change intensities (frames b-f) from the dry initial survey (frame a) in a top-down view of 60-m diameter plot. The depicted image is a ≈ 5-cm thick layer, which was geospatially interpolated immediately atop the alluvium interface. Within the raw radargram data of figure 3, this horizon is identified by the near-right margin arrow. The frames of figure 7 are not radargrams, but instead are difference maps depicting radargram pattern change from the initial dry state (frame a) in 45-min. increments to (frame f). To produce these images, the water application rate to the inner 8-m diameter ring was continuous at ≈ 25 mm/h for the first 2 h, and once water ponding within the ring occurred, was reduced to ≈ 12 mm/h (fig. 6) to maintain constant-state surface ponding for the remainder of the test.

Table 1. GPR System Settings.

Parameter	SIR-20 System Settings
Samples/Scan	512
Bits/Sample	16
Scans/Second	50
Range	100 ns (≈ 4 −5 m)
Range gain	4.0, 59.0, 71.0, 71.0, 73.0 db
Horz IIR Stack	TC = 3
Vert IIR LP N = 2	50 MHz
Vert IIR HP N = 2	600 MHz
Surface speed	7 km/h

In frames b-f of figure 7, a meandering movement of water atop the soil interface can be visualized leaving the central profile beneath the infiltrometer toward the west. The profile appears almost entirely inundated after 2 h (fig. 7, frame f). At north north-east of the center rings were a series of fire ant mounds on the surface along the perimeter of the plot, which were disturbed by the antenna sled. The brighter reds are indicative of the wetting front, as this is where the sharpest change in the dielectric occurs resulting in a strong radar reflection. The light green haze represents saturated soil, a more uniform dielectric and a weaker radar reflector. Water applied at the surface infiltrated 2 m in depth and traveled 30 m laterally in less than 45 min.

Figure 7 exhibits a slight spiral pattern effect, which is most noticeable in frames e and f near the inner ring. This is due to the driving pattern required for the single antenna to cover the width of the spiral path. Three offset tracks of the

single antenna were used to encompass the width of spiral path. Traveling each track about the spiral required 15 minutes. The three tracks were combined to interpolate the surface of each frame of figure 7. Subsurface water was moving at a greater lateral velocity than the survey procedure could sample with a single antenna. To address this interpolation issue, either the spiral path can be narrowed to one antenna width, or a multiple channel, side-by-side antenna array can be towed to obtain both time and spatially contiguous data.

Figure 8 illustrates a three-dimensional image slice of radargram data taken prior to water application. This is the initial state data of figure 6a. The crosshair points to an apparent fissure within the alluvium interface, which is permitting rapid drainage into lower strata. The dynamic presentation of figure 7 assisted in the interpretation of the more complex patterns of figure 8.

Conclusion

Our research team has developed a unique survey protocol that quantifies near-surface preferential flow using GPR, DGPS, and image segmentation based upon dissimilarity. The survey field protocol consists of a mobile GPR system that repeatedly spirals outward along a prescribed course, gathering subsurface data continuously for several hours. After first establishing dry initial-state pattern signatures, metered irrigation begins within a centrally located water-ponding ring. Following vertical infiltration, the water radiates outward from the central application point throughout the subsurface along preferential flow pathways, which are highlighted by GPR. A radargram classifier rapidly segments the profiles by pattern similarities. Within the sequential radargrams, only those specific geo-referenced locales that reveal pattern shifts from the initial state are recognized as being excited by water flow phenomena.

Pattern shifts have been found to highlight the preferential flow channels that occur within the patterns of highly complex radargrams. Sample data are provided showing surface-applied water moving beneath the surface, dropping 2 m in elevation and traveling at lateral velocities of $\approx \times 40$ m/h.

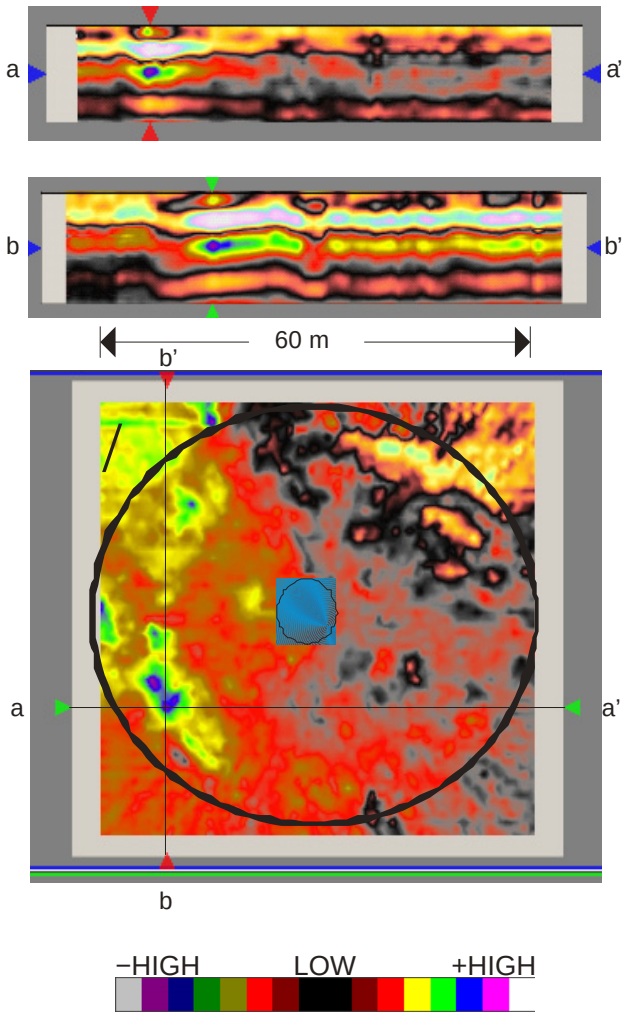

Figure 8. Three-dimensional image slice of radargram data taken prior to water application. Crosshair is at an alluvium interface fissure.

Acknowledgements

The authors gratefully acknowledge the support of The Trustees of the Hobart Ames Foundation, and the staff of Ames Plantation, Grand Junction, Tennessee.

References

Al-Nuaimy, W., Y. Huang, M. Nakhkash, M. T. C. Fang, V. T. Nguyen, and A. Eriksen. 2000. Automatic detection of buried utilities and solid objects with GPR using neural networks and pattern recognition. *J. Appl. Geophy.* 43(2-4): 157-165.

Chanzy, A., A. Tarussov, A. Judge, and F. Bonn. 1996. Soil water content determination using a digital ground-penetrating radar. *Soil Sci. Soc. Am. J.* 60(5): 1318-1326.

Freeland, R. S., J. C. Reagan, R. T. Burns, and J. T. Ammons. 1998. Sensing perched water using ground-penetrating radar–a critical methodology examination. *Applied Engineering in Agriculture* 14(6): 675-681.

Freeland, R. S., D. J. Inman, J. T. Ammons, R. E. Yoder, and L. L. Leonard. 2002a. Detecting vertical anomalies within loessial soils using ground-penetrating radar. *Applied Engineering in Agriculture* 18(2): 263–264.

Freeland, R. S., R. E. Yoder, J. T. Ammons, and L. L. Leonard. 2002b. Integration of real-time global positioning with ground-penetrating radar surveys. *Applied Engineering in Agriculture* 18(5): 647-650.

Gish, T. J., W. P. Dulaney, K. J. S. Kung, C. S. T. Daughty, J. A. Doolittle, and P. T. Miller. 2002. Evaluating use of ground-penetrating radar for identifying subsurface flow paths. *Soil Sci. Soc. Am. J.* 66(5): 1620-1629.

Hardeman, W. D. 1966. Geologic Map of Tennessee (West Sheet). State of Tennessee Department of Conservation, Division of Geology, Nashville, Tenn.

Huisman, J., C. Sperl, W. Bouten, and J. Verstraten. 2001. Soil water content measurements at different scales: Accuracy of time domain reflectometry and ground penetrating radar. *J. Hydrol.* (Amsterdam) 245(1): 48-58.

Huisman, J., S. Hubbard, J. Redman, and A. Annan. 2003. Measuring soil water content with ground penetrating radar: A review. *Vadose Zone J.* 2(4): 476-491.

Inman, D. J., R. S. Freeland, J. T. Ammons, and R. E. Yoder. 2002. Soil Investigations using electromagnetic induction and ground-penetrating radar in Southwest Tennessee. *Soil Sci. Soc. Am. J.* 66(1): 206-211.

Lu, Q., and M. Sato. 2002. Groundwater monitoring by GPR in Mongolia. *Proc. of SPIE, Ninth International Conference on Ground Penetrating Radar*, eds. S. Koppenjan and H. Lee, 545-550. Bellingham, Wash.: SPIE.

Lunt, I. A., S. S. Hubbard, and Y. Rubin. 2005. Soil moisture content estimation using ground-penetrating radar reflection data. *J. Hydrol.* 307(2005): 254-269.

Nakashima, Y., H. Zhou, and M. Sato. 2001. Estimation of groundwater level by GPR in an area with multiple ambiguous reflections. *J. Appl. Geophys.* 47(3): 241-249.

Odhiambo, L. O., R. S. Freeland, R. E. Yoder, and J. W. Hines. 2004. Investigation of a fuzzy neural network application in classification of soils using ground penetrating radar imagery. *Applied Engineering in Agriculture* 20(1): 109-117.

Shih, S. F., J. A. Doolittle, D. L. Myhre, and G. W. Schellentrager. 1986. Using radar for groundwater investigation. *J. Irrig. Drain. E-ASCE* 112(2): 110-118.

Shihab, S., W. Al-Nuaimy, and Y. Huang. 2002. Neural network target identifier based on statistical features of GPR signals. *9th Intern. Conf. on Ground Penetrating Radar, Proceedings of SPIE*, 135-138. Bellingham, Wash.: SPIE.

Trinks, I., D. Wachsmuth, and H. Stümpel. 2001. Monitoring water flow in the unsaturated zone using georadar. *First Break* 19(12): 679-684.

van Overmeeren, R. A., S. V. Sariowan, and J. C. Gehrels. 1997. Ground penetrating radar for determining volumetric soil water content; results of comparative measurements at two sites. *J. of Hydrol*. 197(1/4): 316-338.

Vellidis, G., M. C. Smith, D. L. Thomas, and L. E. Asmussen. 1990. Detecting wetting front movements in sandy soil with ground-penetrating radar. *Transactions of the ASAE* 33(6): 1867-1874.

Weiler, K., T. Steenhuis, J. Boll, and K.-J. Kung. 1998. Comparison of ground penetrating radar and time domain reflectometry as soil water sensors. *Soil Sci. Soc. Am. J.* 62(5): 1237-1239.